

Using complex networks towards information retrieval and diagnostics in multidimensional imaging

Soumya Jyoti Banerjee¹, Mohammad Azharuddin², Debanjan Sen³, Smruti Savale³, Himadri Datta³, Anjan Kr Dasgupta², and Soumen Roy^{1,*}

¹Bose Institute, 93/1 Acharya PC Roy Road, Kolkata 700 009, India

²Department of Biochemistry, University of Calcutta, 35 Ballygunge Circular Road, Kolkata 700 019, India

³Regional Institute of Ophthalmology, Calcutta Medical College and Hospital, Kolkata 700 073, India

*soumen@jcbose.ac.in

ABSTRACT

We present a fresh and general yet simple approach towards information retrieval in general and diagnostics in particular by applying the theory of complex networks on multidimensional images. We demonstrate a successful use of our method with the time series generated from high content thermal imaging videos of patients suffering from aqueous deficient dry eye (ADDE) disease. The approach is scalable to a device where fluctuation derived network parameters serve as diagnostic markers. Remarkably, network analysis of thermal imaging time series of contact lens users and patients upon whom Laser-Assisted in situ Keratomileusis (Lasik) surgery has been conducted, exhibits pronounced similarities with results obtained from ADDE patients. We also propose a general framework for transformation of multidimensional images to networks for futuristic biometry.

Introduction

What is the use of all knowledge if it is inaccessible? Indeed, this feeling echoes in the ACM SIGMM grand challenge to “make capturing, storing, finding, and using digital media an everyday occurrence in our computing environment”¹. Content Based Image Retrieval (CBIR) started with retrieval of specific images and videos from large arrays of images or videos. Nowadays, CBIR is more generally referred to as Content Based Multimedia Information Retrieval (CBMIR) or simply MIR. Information retrieval in general can be conceived of as finding material of an unstructured nature that satisfies an information need from within large collections². Applications of pictorial search into a database of images already existed in specialized fields like character recognition, face recognition, and, robotic guidance. IBM developed the first commercial CBIR system, called QBIC (Query by Image Content) in 1995³. At present, the basic problem is the creation of powerful content-based methods in order to enable or improve multimedia retrieval. Many interesting and challenging scenarios arise in case of real time videos, e.g. surveillance, live cell imaging in life sciences, biomedical imaging etc.

Multidimensional imaging (MDI) is a ubiquitous and integral part of modern life. It is used in extremely diverse fields ranging from entertainment or surveillance on one hand to science, medicine or surgery on the other. To thrive like any other successful technology, a typical MDI technique needs to be inexpensive, portable, robust and high resolution to the extent possible. Additionally, successful coupling with information retrieval algorithms could yield substantial premium. In this context, thermal imaging (TI) occupies an important place in MDI. TI is an economical and potent yet relatively unexplored technique in medical diagnostics. Lower imaging resolution and variability of steady state thermal behavior due to environmental thermal fluctuations are seen as primary reasons for the restrictive use of this powerful non-invasive method.

The process of conversion of any given video to a time series has been known for some time⁴. Albeit, to our knowledge, the fullest potential of this conversion in thermal imaging has not been exploited. Also, the network representation of time series, provides us with an analytical tool that may allow object identification, not possible by conventional image processing technique. The uniqueness in this identification approach is use of time instead of spatial distribution based analysis. Effective utilisation of the vast research in time series analysis and related advances is obviously critical to gain liberal advantage of this transformation in information retrieval. As such network based insights can be fed back for extraction of hidden image contents which are evident from the spatial data alone.

A large number of approaches to analyze time series have been proposed over time. These range from time-frequency methods, such as Fourier and wavelet transforms⁵⁻⁷, to nonlinear methods, such as phase-space embeddings, Lyapunov exponents, correlation dimensions and entropies⁸⁻¹⁰. These techniques are helpful for summarizing the characteristics of a time

series into compact metrics. Such brevity can be efficiently exploited to effectively understand the dynamics or to predict how the system will evolve over time. However, these measures preserve many but not all of the important properties of a given time series. Therefore, there is considerable research toward the identification of metrics that can capture the additional information or quantify time series in a completely new ways¹¹⁻¹⁴.

Quite independent of the above, the field of complex networks has been extensively studied by itself and successfully applied in manifold instances in science, nature and engineering^{15,16}. With significant advances being reported from various fields¹⁷⁻²⁶, the importance of converting time series into networks is becoming increasingly clear over the last few years²⁷.

In this work, we furnish a new, simple and general route to information retrieval by combining developments from all these disparate fields and show that such an approach can yield rich dividends for MDI in general and for diagnostics in particular. Indeed, following the broad framework proposed here, it is possible to construct inexpensive devices for non-invasive diagnostics and biometric based applications, which can perform successfully in real-time²⁸. Our method consists of the following steps: (i) conversion of a given video or MDI into time series, (ii) conversion of the time series into a network, and finally (iii) analysing the network metrics to identify specific topological metric/(s) which can act as good discriminators for different videos. Obviously, dimension reduction achieved by our method would make feature identification of complex videos and images computationally far simpler. As detailed below, our approach effectively opens up the avenue of fluctuation based diagnostics in biomedical MDI. Hardware implementations of this method would be extremely versatile, as it is smart, fast and portable²⁸.

While the approach proposed in this paper is very general, here we specifically concentrate on patients with Aqueous Deficient Dry Eye (ADDE) disease, contact lens users and patients who have undergone Lasik operations. We also investigate applications of our work in biometrics. ADDE is a disturbance in tear film physiology that leads to various abnormal states of ocular surface cells that elevate the incidence of ocular surface disorders and infection. ADDE represents one of the most common ocular pathologies and is a complex multifactorial disease characterized by an immune and inflammatory process that affects the lacrimal glands and ocular surface. Its diagnosis by assessment of the tear film has been extensively studied²⁹⁻³¹. Most of the diagnostic approaches are based on either osmolarity or evaporation of the tear film. Studies indicate that most ADDE measures do not capture the etiologies for dry eye, such as dysfunctional neurology, hormonal influences or the inflammatory nature of the condition. Another situation that may affect the alteration of the tear dynamics is the use of contact lens. Statistical studies of thermal fluctuation of healthy individuals (control) and ADDE patients where non-invasive TI was used, have been conducted recently³². Significant correlation of thermal fluctuations is found between left and right eye of control whereas this property is completely absent in eyes of ADDE patients. However, the problem of classification of dry eye either from collective or individual data remains unsolved. Also, parametric classification to differentiate or diagnose healthy and dry eye individuals is still unavailable. The mechanism proposed here shows that thermal fluctuation based approaches and a robust parametrization of such fluctuation by network mapping may be a powerful alternative approach to express the etiology of the eye. Throughout this paper, we use the terms dry eye and ADDE interchangeably. However, it should be especially noted that in medical literature, ADDE denotes only one of the spectra of alteration of ocular surfaces going by the name of the dry eye.

Methods

Thermal Imaging Videos. For our experiments, we used a Forward Looking Infra Red (FLIR) thermal camera (Model no. FLIR SC 305, FLIR Systems AB, Sweden). We obtained TI videos of 15 second duration for the facial portion of 42 dry eye patients and 29 regular contact lens users. For the latter class, videos were separately acquired for every individual when he or she was (a) wearing the lens, and, (b) not wearing the lens. The facial videos obviously include both left and right eyes and cheeks. An almost equal number of 36 individuals with healthy eyes (control) were also studied for the same duration of 15 second. Only videos where subjects have not blinked their eye during the duration of imaging have been considered in this work.

Conversion of Videos to Time Series. The video obtained in the FLIR setup is converted to AVI format. The AVI file is then subjected to frame wise decomposition. Each frame is then cropped to select a region of interest (say eye, cheek etc). The average pixel for the region of interest is then evaluated at a given time. Thus, a time series of N points can be obtained, where each point represents the average instantaneous temperature of the selected region, $\tau(t)$, at time instant, t . The initial instantaneous temperature, $\tau(0)$, at $t = 0$, is then set to 0. Thence, we obtain our final time series, $X(t) = \tau(t) - \tau(0)$.

Detrending and Pooling Time Series. Some linear trend from decay of eye temperature is likely to be present in the time series generated from every video due to evaporation of water from the eye. In the event, that a large single time series is generated by pooling each of these smaller time series, a pseudo-periodicity could be created, which could mislead our predictions. So we detrend each time series separately to strip the accumulated time series from such a linear trend and normalize it by mean

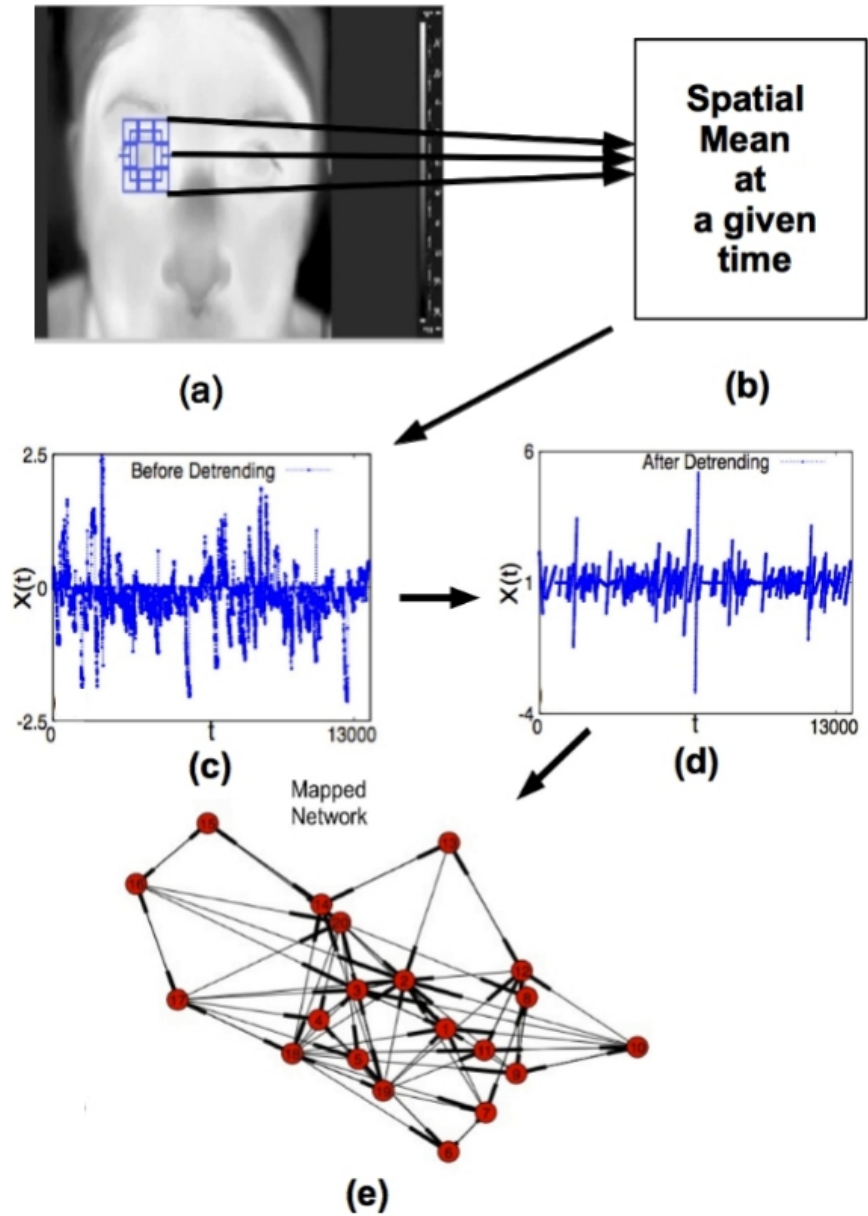


Figure 1. (a) Thermal imaging of the right eye of an arbitrary individual, (b) spatial mean of the cropped region of interest at time t . Plot of pooled thermal time series data for both eyes of a particular group (like dry eye patients or healthy individuals) of all such thermal images (c) before detrending, and, (d) after detrending. Directed network obtained from mapping of detrended time series is shown in (e).

of all detrended values to fixed amplitude base line as shown in Figs. 1(a) and 1(b). We independently pool the time series data of (a) both left and right eyes collectively, and, (b) the cheek of every individual in a given eye group (control or dry) and create a single time series. In all, we have eight classes of pooled time series. Throughout the rest of the paper, we often use $\{\mathcal{H}_e\}, \{\mathcal{D}_e\}, \{\mathcal{H}_c\}, \{\mathcal{D}_c\}, \{\mathcal{C}_L\}, \{\mathcal{C}_N\}, \{\mathcal{L}_B\}$ and $\{\mathcal{L}_A\}$ to denote: (i) healthy eyes (control group), (ii) dry eye group, (iii) cheek (control group), (iv) cheek (dry eye group), (v) group of contact lens users wearing lens, (vi) group of contact lens users not wearing lens, (vii) group of patients who underwent Lasik operations - before the procedure, and, (viii) group of patients who underwent Lasik operations - after the procedure. It should be noted that the individuals in (i) $\{\mathcal{C}_L\}$ and $\{\mathcal{C}_N\}$, and, (ii) $\{\mathcal{L}_B\}$ and $\{\mathcal{L}_A\}$ are identical.

Creation of Networks from Time Series: Background. In literature, there are a few interesting approaches for time series to network mapping, based on different concepts such as correlations,^{33,34} visibility,^{35,36} recurrence analysis,³⁷ transition probabilities^{38–40} and phase-space reconstructions.^{41,42} A complete list of all the proposed maps can be found in Donner et al.⁴³ and references therein. These studies are able to capture that distinct properties of a time series can be mapped onto networks with distinct topological properties. These findings claim that it may be possible to differentiate different time series features using network metrics. But it was unclear as to how these network topological properties are related to the original time series. The main drawback of these maps $M : T \rightarrow G$ from the time series domain T to the network domain G however, is that they do not have a natural inverse mapping $M^{-1} : G \rightarrow T$. Recently, some researchers have tried to construct an inverse map.^{27,40,44} Nonetheless, these methods are either sensitive to arbitrarily chosen parameters^{27,44} or are dependent on the information about the given map M for construction of an inverse mapping M^{-1} .⁴⁰ Therefore, they are not immensely useful for real world networks, when M is not known in advance. Here we have used a completely new time series to network mapping technique,²⁷ which is dual in nature i.e. this mapping approach has a natural and robust inverse map. This fully invertible map makes it possible to create a “dual” representation of a time series and its corresponding network counterpart and directly relates common network statistics back to the original time series and vice-versa. Using this method, time series can be mapped to a directed network.²⁷

Mapping Time Series to Directed Networks. We have followed methods well-established in literature⁴⁵, for mapping the detrended time series of each of the eight groups mentioned above, namely, $\{\mathcal{H}_e\}, \{\mathcal{D}_e\}, \{\mathcal{H}_c\}, \{\mathcal{D}_c\}, \{\mathcal{C}_L\}, \{\mathcal{C}_N\}, \{\mathcal{L}_B\}$ and $\{\mathcal{L}_A\}$, into eight distinct directed networks. These directed networks are denoted by $G_i(\mathcal{V}_i, \mathcal{E}_i)$, where, \mathcal{V}_i and \mathcal{E}_i is the set of all nodes and edges respectively in network, and, $i \in \{\{\mathcal{H}_e\}, \{\mathcal{D}_e\}, \{\mathcal{H}_c\}, \{\mathcal{D}_c\}, \{\mathcal{C}_L\}, \{\mathcal{C}_N\}, \{\mathcal{L}_B\}, \{\mathcal{L}_A\}\}$. Further, for our case, we divide the Y-axis of Fig. 1(d) into 20 quantiles. In our analysis, we have ignored the edge weights because we are more interested in capturing important thermal fluctuation transitions from one quantile to another and not in how many times such transitions occurred.

Analyzing Directed Networks. All directed networks, thus obtained by mapping from thermal time series have been analyzed thoroughly using most known network metrics²². However, among all of them, we find that edge betweenness centrality^{21,25}, \mathcal{B}_e , demonstrates significant discriminating power, a fact that can well be exploited to construct a functional device²⁸. For directed networks, \mathcal{B}_e , $e \in \mathcal{E}_i$ is the ratio of the number of directed shortest paths, $\sigma(s, t|e)$, between node, s , and node, t , which pass through edge, e , and the total number of directed shortest paths, $\sigma(s, t)$, between node, s , and node, t , in the network. Mathematically, it is defined as:

$$\mathcal{B}_e = \sum_{s \neq t} \frac{\sigma(s, t|e)}{\sigma(s, t)} \quad (1)$$

We then construct the *cumulative distribution* of \mathcal{B}_e , for each of the above groups.

Results

Cumulative Edge Betweenness Centrality Distribution for Dry Eye Versus Healthy Eye. From the cumulative \mathcal{B}_e distributions shown in Fig. 2 it is clear that the networks mapped from pooled TI time series of eye for healthy eyes (control) group, $\{\mathcal{H}_e\}$, possess lower \mathcal{B}_e values whereas the networks mapped from pooled TI time series of eye for dry eyes group, $\{\mathcal{D}_e\}$, possess higher \mathcal{B}_e values. Since dry eye is a pathology of the eye; from Fig. 2 we get a hint that presence of edges with high \mathcal{B}_e value could possibly be a suitable distinguishing, diagnostic feature for multiple pathological conditions in eyes. We subsequently find that this is indeed true to a large measure.

Diagnosing Patients with Dry Eye. As aforementioned thermal imaging videos of 15 second duration were obtained for 42 dry eye patients, 36 healthy individuals and 29 regular contact lens users. In addition, TI videos of healthy individuals and

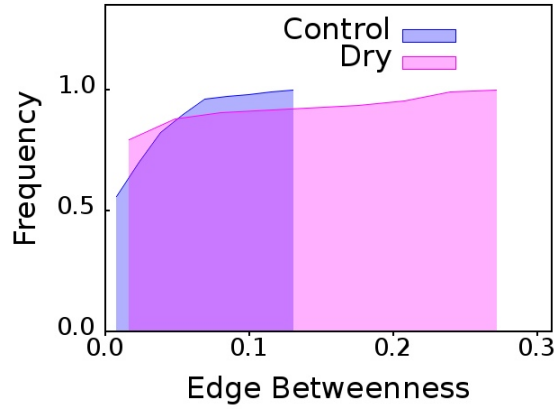


Figure 2. Cumulative distribution of edge betweenness centrality for networks mapped from pooled thermal imaging time series for healthy eye and dry eye groups.

patients with dry eye were further recorded for independent validation. These “test case” videos were of a total duration of 1 minute and obtained by pooling TI Videos of 15 second duration of the same individual. Such pooling is necessary, because: (i) blinking of eyes is not allowed in our experiment and it is difficult for most individuals not to blink even once in a minute, and, (ii) proper rest needs to be given to the eyes of all participants in the experiment.

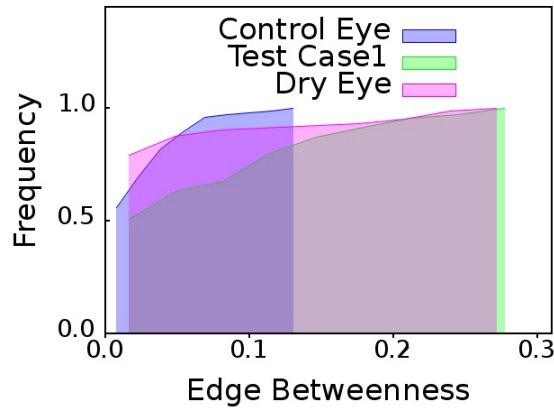


Figure 3. Cumulative distribution of edge betweenness centrality, \mathcal{B}_e , for networks mapped from pooled thermal imaging time series for individuals with healthy eyes (control) and dry eye patients shown in Fig. 2 and a test case. The test case is that of a dry eye patient whose cumulative \mathcal{B}_e distribution is almost identical to the cumulative \mathcal{B}_e distribution of networks mapped from pooled thermal imaging time series data for all other dry eye patients.

From the cumulative \mathcal{B}_e distributions shown in Fig. 3, we observe that cumulative \mathcal{B}_e distribution of test case 1 eye individual has larger shift toward right. The network mapped from TI time series for test case 1 eye network has larger number of edges with high \mathcal{B}_e values which is quite similar to dry eye group. On the other hand, in the network obtained for test case 2 eye individual, the \mathcal{B}_e distribution is akin to that of the control eyes group as seen in Fig. 4. Therefore, we can reasonably infer that test case 1 should be a dry eye and test case 2 should be a healthy eye. Thus, in practice, diagnosis of dry eye is indeed possible by non-invasive thermal imaging of the eye of the patient for 60 second, by sufficiently resting the eyes of the arbitrary individual after every 15 second.

Contact Lens Users. From the cumulative distributions shown in Fig. 5, it is clear that the groups of contact lens users, (a) who are wearing lens, $\{\mathcal{L}_\varphi\}$, and, (b) who are not wearing lens, $\{\mathcal{L}_\mathcal{N}\}$; show characteristics similar to the dry eye group, $\{\mathcal{D}_e\}$, i.e., presence of edges with high \mathcal{B}_e values when compared to the group of healthy individuals, $\{\mathcal{H}_e\}$. Contact lens

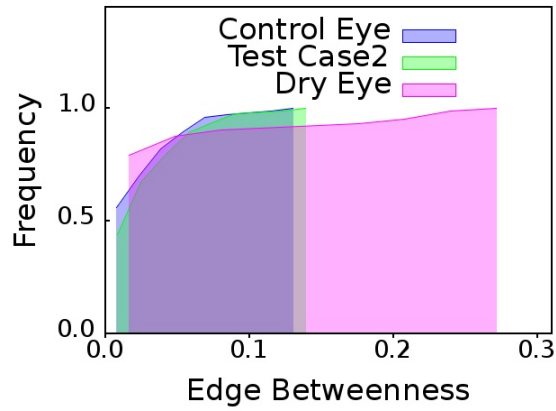


Figure 4. Cumulative distribution of edge betweenness centrality, \mathcal{B}_e , for networks mapped from pooled thermal imaging time series for individuals with healthy eyes (control) and dry eye patients shown in Fig. 2 and a test case. The test case is that of a healthy individual whose cumulative \mathcal{B}_e distribution is almost identical to the cumulative \mathcal{B}_e distribution of networks mapped from pooled thermal imaging time series data for all healthy individuals.

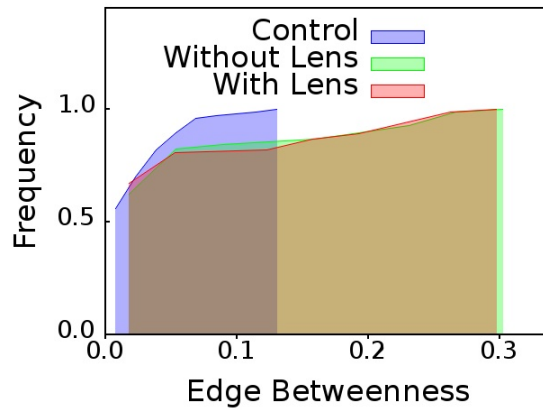


Figure 5. Cumulative distributions of edge betweenness centrality, \mathcal{B}_e for networks mapped from pooled thermal imaging time series for individuals with healthy eyes, $\{\mathcal{H}_e\}$, and contact lens users. For the latter category, thermal imaging was conducted when they were : wearing their contact lens, $\{\mathcal{C}_L\}$, and not wearing their contact lens $\{\mathcal{C}_N\}$.

users obviously also have unhealthy eyes due to myopia or hypermetropia. Significantly, removal of contact lens has almost no effect on the nature of the distribution.

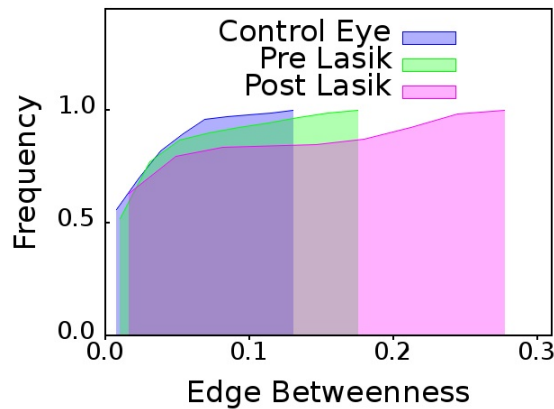


Figure 6. Cumulative distributions of edge betweenness centrality, \mathcal{B}_e for networks mapped from pooled thermal imaging time series for individuals with healthy eyes, $\{\mathcal{H}_e\}$, and Lasik eyes. Thermal imaging was conducted on the latter category, both, (a) before they underwent surgery, $\{\mathcal{L}_B\}$, and after they underwent surgery, $\{\mathcal{L}_A\}$.

Patients Undergoing Lasik surgery From the cumulative \mathcal{B}_e distributions shown in Fig. 6, we observe that cumulative \mathcal{B}_e distribution of patients who have undergone Lasik surgery is also very similar to that of the cumulative \mathcal{B}_e distribution of dry eye group; just like the case of contact lens users.

Biometric applications. To identify possible biometric applications from our method, we also investigated the thermal fluctuations of other portions of the face apart from the eyes, namely, the cheek. The very same facial videos of both control eye and dry eye groups were studied for this purpose. This time however, the cheek portion was selected. 15 identical individuals were randomly selected from $\{\mathcal{H}_e\}$ and $\{\mathcal{H}_c\}$. Similarly, 15 identical individuals were also randomly selected from $\{\mathcal{D}_e\}$ and $\{\mathcal{D}_c\}$. We *independently* pooled 15 detrended thermal times series, obtained from cheek and eye TI time series data for $\{\mathcal{H}_e\}$, $\{\mathcal{H}_c\}$, $\{\mathcal{D}_e\}$ and $\{\mathcal{D}_c\}$.

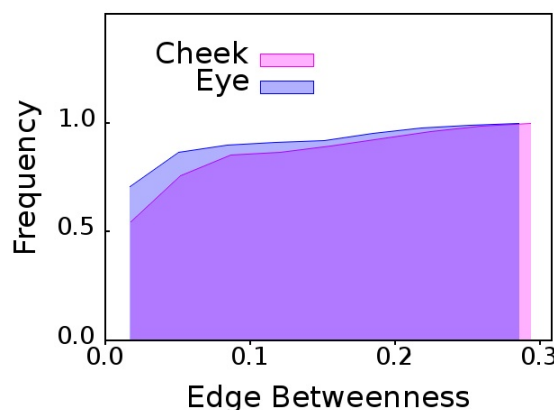


Figure 7. Cumulative distributions of edge betweenness centrality, \mathcal{B}_e of networks mapped from pooled thermal imaging time series for 15 individuals with dry eyes, and, their cheeks

Very interestingly, the cumulative edge betweenness, \mathcal{B}_e , distributions for eye and cheek show completely different behavior. In the former case, the cumulative \mathcal{B}_e distribution of individuals with dry eyes selected from $\{\mathcal{D}_e\}$ and $\{\mathcal{D}_c\}$ are almost identical, as can be observed from Fig. 7. However, in the latter case, cumulative \mathcal{B}_e distribution of individuals with healthy

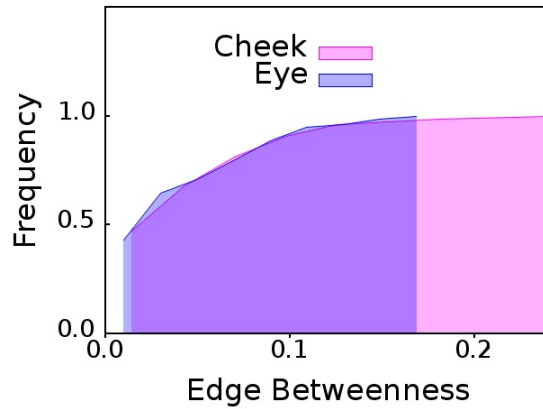


Figure 8. Cumulative distributions of edge betweenness centrality, \mathcal{B}_e of networks mapped from pooled thermal imaging time series for 15 individuals with healthy eyes, and, their cheeks

eyes selected from $\{\mathcal{H}_e\}$ and $\{\mathcal{H}_c\}$ are very different, as visible in Fig. 8.

The above observations are extremely important from the biometrics point of view for the following reasons. If there is any metabolic or functional object in which a biochemical or chemical activity is in progress, the temporal data transformed in network can provide a parametric identification of the status of the process, and the regional dependence of the same can further provide information regarding aberrations in functional status if any.

Discussion

The present method has an inbuilt potential for incorporating a distance based measure for object identification. In this work however, a distance based measure is not introduced because the results have already been very clearly segregated.

Edges of the directed networks represent the transitions from one temperature range to another; for example from a lower temperature regime to higher temperature regime or vice versa. For this reason, edge based network metrics would be very suitable for classification of thermal time series. Thus, it is not a surprise that edge betweenness centrality, \mathcal{B}_e , captures the most important transitions, representing significant thermal fluctuations, between two completely different temperature regimes, and, in the process exhibits such clear discriminating properties.

The results presented here illustrate that network based high content imaging can be a powerful tool for classification of objects in an image. The discriminatory potential of the said approach, which is in full display for: ADDE patients in Fig. 2, Lasik patients in Fig. 6 and contact lens users in Fig. 5; can hardly be derived using conventional video processing techniques.

An additional challenging task, namely thermal segmentation may also be performed. In conventional imaging, segmentation implies separating the object and the background. In thermal imaging background, we can use the environmental thermal fluctuations. Notably, when eyes and cheek are studied together, the discrimination occurs only in control eyes and not in diseased eyes. This would have interesting prognostic implications. The fact that the fluctuation patterns of the eyes of dry eye patients are similar to their cheeks, implies that the environmental fluctuations of temperature plays a more conspicuous role for them. For the healthy individuals on the other hand, the inherent metabolism of the eye has its own signature. The cheek in this case actually serves as a thermal background.

While the immediate diagnostic potential of our findings for contact lens users or Lasik operated patients is unclear, the remarkable similarity of the cumulative \mathcal{B}_e distribution for all eye diseases investigated here, namely, ADDE, contact lens users who obviously suffer from myopia or hypermetropia and Lasik operated patients is indeed striking. The last finding is specially interesting in context of the ongoing debate in ocular medicine as to whether Lasik operation actually leads to deterioration in the condition of the patients eye.

Last and certainly not the least, for future scope, it may be noted that network based imaging approach can be exploited for designing efficient alert systems or biometric codes. Similarly, the technique can be applied to other forms of non-thermal high content imaging. The temporal dynamics provides us a toolbox that would serve to compliment the knowledge gained from conventional image processing.

References

1. Rowe, L. A. & Jain, R. ACM SIGMM report on future directions in multimedia research. *ACM Trans. Multimedia Computing, Communications, and Application* **1**, 3-13 (2005).
2. Manning, C. D., Raghavan, P. & Schütze, H., *Introduction to Information Retrieval* (Cambridge University Press, 2008).
3. Flickner, M. *et al.* Query by image and video content: the QBIC system. *IEEE Computer* **28**, 23-32 (1995).
4. Ishihara, K., Kawagoe, M. & Hasegawa, R. Apparatus for and method of extracting time series image information. US Patent 5953439 (1999).
5. Korner, T. W. *Fourier Analysis* (Cambridge University Press, 1988).
6. Box, G. E. P., Jenkins, G. M. & Reinsel, G. C. *Time Series Analysis: Forecasting and Control* (John Wiley & Sons, Inc., 2008).
7. Percival, D. B. & Walden, A. T. *Wavelet Methods for Time Series Analysis* (Cambridge University Press, 2006).
8. Strogatz, S. H. *Nonlinear Dynamics And Chaos: With Applications To Physics, Biology, Chemistry, And Engineering* (Perseus Books Group, 1994).
9. Kantz, H. & Schreiber, T. *Nonlinear Time Series Analysis* (Cambridge University Press, 2003).
10. Campanharo, A. S. L. O *et al.* Searching chaos and coherent structures in the atmospheric turbulence above the Amazon forest. *Phil Trans R Soc A* **366**, 579-589 (2008).
11. Zhang, J. & Luo, X., Small, M. Detecting chaos in pseudoperiodic time series without embedding. *Phys. Rev. E* **73**, 016216 (2006).
12. Lai, C., Chung, P. & Tseng, V. S. A novel two-level clustering method for time series data analysis. *Expert Systems with Applications* **37**, 6319-6326 (2010).
13. Verplancke, T. *et al.* A novel time series analysis approach for prediction of dialysis in critically ill patients using echo-state networks. *BMC Medical Informatics and Decision Making* **10**, 1-7 (2010).
14. Ao, S. *Applied Time Series Analysis and Innovative Computing* (Springer, 2010).
15. Albert, R. & Barabási, A. L. Statistical mechanics of complex networks. *Rev. Mod. Phys.* **74**, 47 (2002).
16. Newman, M. E. J. *Networks: An Introduction* (Oxford Univ. Press, UK, 2010).
17. Buldyrev, S. V., Parshani, R., Paul, G., Stanley, H. E. & Havlin S. Catastrophic cascade of failures in interdependent networks. *Nature* **464**, 1025-1028 (2010).
18. Roy, S. & Filkov, V. Strong associations between microbe phenotypes and their network architecture. *Phys. Rev. E* **80**, 040902(R) (2009).
19. Dorogovtsev S. N., Goltsev A. V. & Mendes J. F. F. Critical phenomena in complex networks. *Rev. Mod. Phys.* **80**, 1275 (2008).
20. Wuellner, D. R., Roy, S. & D'Souza R. M. Resilience and rewiring of the passenger airline networks in the United States. *Phys. Rev. E* **82**, 056101 (2010).
21. Newman, M. E. J., Girvan, M. Finding and evaluating community structure in networks. *Phys. Rev. E* **69**, 026113 (2004).
22. Filkov V *et al.* Modeling and verifying a broad array of network properties. *Euro. Phys. Lett.* **86**, 28003 (2009).
23. Dandekar, A. M. *et. al.* Analysis of early host responses for asymptomatic disease detection and management of specialty crops. *Crit. Revs. Immunol.* **30**, 277-289 (2010).
24. Roy, S. Systems biology beyond degree, hubs and scale-free networks: the case for multiple metrics in complex networks. *Syst. Synth. Biol.* **6**, 31-34 (2012).
25. Girvan, M. & Newman, M. E. J. Community structure in social and biological networks. *PNAS USA* **99**, 7821-7826 (2002).
26. Banerjee, S. J., Sinha, S. & Roy, S. Slow poisoning and destruction of networks: Edge proximity and its implications for biological and infrastructure networks. *Phys. Rev. E* **91**, 022807 (2015).
27. Strozzi, F., Zaldívar, J. M., Poljansek, K., Bono, F. & Gutiérrez, E. From complex networks to time series analysis and viceversa: Application to metabolic networks. *JRC Scientific and Technical Reports, EUR* **23947**, JRC52892 (2009).
28. Roy, S. *et al.* A system and method for analyzing videos of application or function for feature identification of the videos and related application or function. Indian Patent 628/KOL/2015 filed June 03, (2015).

29. Tomilson, A. & Khanal, S. Assessment of Tear Film Dynamics: Quantification Approach. *Clinical Science* **3**, 81-95 (2005).
30. Khanal, S., Tomlinson, A., McFadyen, A., Diaper, C. & Ramaesh, K. Dry Eye Diagnosis. *Investigative Ophthalmology & Visual Science Cornea* **49**, 1407-1414 (2008).
31. Goins, K. M. New Insights into the Diagnosis and Treatment of Neurotrophic Keratopathy. *The Ocular Surface* (Elsevier) **3**, 96-110 (2005).
32. Azharuddin M., Bera S. K., Datta H. & Dasgupta, A. K. Thermal fluctuation based study of aqueous deficient dry eyes by non-invasive thermal imaging. *Experimental Eye Research* (Elsevier) **120**, 97-102 (2014).
33. Zhang, J. & Small, M. Complex network from pseudoperiodic time series: Topology versus dynamics. *PRL* **96**, 238701 (2006).
34. Yang, Y. & Yang, H. J. Complex network-based time series analysis. *Physica A* **387** (2008).
35. Lacasa, L., Luque, B., Ballesteros, F., Luque, J. & Nuno, J. C. From time series to complex networks: The visibility graph. *PNAS USA* **105**, 4972-4975 (2008).
36. Luque, B., Lacasa, L., Ballesteros, F., Luque, J. Horizontal visibility graphs: Exact results for random time series. *Phys. Rev. E* **80**, 046103 (2009).
37. Marwan, N., Donges, J. F., Zou, Y., Donner, R. V. & Kurths, J. Complex network approach for recurrence analysis of time series. *Physics Letters A* **373**, 4246-4254 (2009).
38. Nicolis, G., Cantu, A. G. & Nicolis, C. Dynamical aspects of interaction networks. *Int. J. Bifurcation Chaos* (World Scientific) **15**, 3467 (2005).
39. Li, P. & Wang, B. H. Extracting hidden fluctuation patterns of Hang Seng stock index from network topologies. *Physica A* **378**, 519-526 (2007).
40. Shirazi, A. H. *et al.* Mapping stochastic processes onto complex networks. *Journal of Statistical Mechanics: Theory and Experiment* **07**, P07046 (2009).
41. Xu, X., Zhang, J., Small, M. Superfamily phenomena and motifs of networks induced from time series. *PNAS USA* **105**, 19601-19605 (2008).
42. Gao, Z., Jin, N. Complex network from time series based on phase space reconstruction. *Chaos* **19**, 033137 (2009).
43. Donner, R. V. *et al.* Recurrence- based time series analysis by means of complex network methods. *Intl J Bifurcation and Chaos* **21**, 1019-1046 (2011)
44. Haraguchi, Y., Shimada, Y., Ikeguchi, T. & Aihara, K. Transformation from complex networks to time series using classical multidimensional scaling. (In: ICANN ' 09: Proceedings of the 19th International Conference on Artificial Neural Networks Heidelberg, Berlin: Springer-Verlag, 2009).
45. Campanharo, A. S. L. O., Simer, M. I., Malmgren, R. D., Ramos, F. M., Amaral, L. A. N. Duality between Time Series and Network. *PLoS ONE* **6**, e23378 (2011).

Acknowledgments

SJB and MA thank Council of Scientific and Industrial research, India and University Grants Commission, India respectively for financial support.

Author Contributions

SR and ADG designed research. SR wrote the manuscript. SJB conducted theoretical analysis. MA conducted the thermal imaging experiments. DS, SS and HD provided clinical supervision.